# Transmission enhancement via metasurfaces with tunable waveband performance by dewetting and seeded masking

Benjamin A. Vaca, Jude K. Yoshino, Tyler A. Benge, William E. Genet, Ishwar D. Aggarwal, and Thomas C. Hutchens\*

Department of Physics and Optical Science, University of North Carolina at Charlotte, 9201 University City Blvd, Charlotte, NC, USA 28223

## **ABSTRACT**

This study demonstrates the fabrication of tunable masking layer consisting of gold islands on fused silica substrates. The goal is to produce anti-reflective structured surfaces (ARSS) that correlate to the repeatable and scalable masking step. The transmission enhancement waveband of fused silica is controlled by variations in gold masking islands created through repetitive dewetting process. Gold layer is formed by physical vapor deposition and thermal annealing. Varying deposition thickness and annealing temperature, size and periodicity of gold islands is controlled. With each iterative step of deposition and annealing, relative periodicity established by the initial island formation, or "seed", is maintained while increasing fill factor in subsequent iterations. Optical transmission spectra were analyzed of the masking layer and formation of metasurface by plasma etching. Results showed that larger deposition thicknesses required higher annealing temperatures to generate circular islands. The seed layer sets the mask periodicity, then the mask fill factor can be increased to allow for deeper etching of ARSS features, for broadband performance. For example, initial deposition thickness of 10 nm and repeated iterative steps of deposition and annealing, the fill factor increased (28%, 39%, 47%, 49%), while the island periodicity was maintained at average 91 ± 6 nm for all iterative steps. Etching these masked samples resulted in broadband transmission enhancement, over 94% of theoretical maximum. A comprehensive database of masking layer fabrication, resultant surface feature dimensions, and ARSS transmission enhancement capabilities was generated. This scalable masking approach can broaden high laser damage threshold applications utilizing tunable performance ARSS.

**Keywords:** anti-reflective, transmission enhancement, metasurface, dewetting, masking, high laser damage threshold, ARSS, random

# 1. INTRODUCTION

## 1.1 Anti-reflection treatments

When light is incident on a surface boundary between two mediums with different refractive indexes, some portion of the light is reflected off the boundary. The reflected light from a smooth surface can be calculated by Fresnel equations and can be detrimental in various applications. Anti-reflective (AR) coatings with multi-layer thin-films can be used to reduce the reflections for a wide range of wavelengths or incident angles. These films can be very effective as they can suppress Fresnel reflections to nearly zero [1]. However, AR coatings have material limitations and suffer from laser damage and delamination when used in very high energy or power applications [2].

The need for optical components to withstand a high energy laser damage threshold (LDT) is crucial in modern laser systems. Thermal effects and the need for index matching make the implementation of thin-film AR coatings increasingly more difficult as energy levels of the laser system are increased [3]. This can be mitigated and significantly improved by fabricating anti-reflective structured surfaces (ARSS) on the optic as opposed to adding multi-layered dielectric or sol-gel coatings [4]. This metasurface is directly etched into the substrate material, creating a dependency on the nano-scale unit structure rather than the materials themselves to limit undesired absorption and reflections. The features are typically on the scale of half the wavelength of operation, acting as a gradual index of refraction change from environment to substrate, or "moth eye" effect [5]. Figure 1 provides an example of how the refractive index changes at each interface for these thin film AR coatings, compared to that of the ARSS. Notice the gradual shift in index for the ARSS features.

\*thomas.hutchens@charlotte.edu; phone 1 704 687 8147

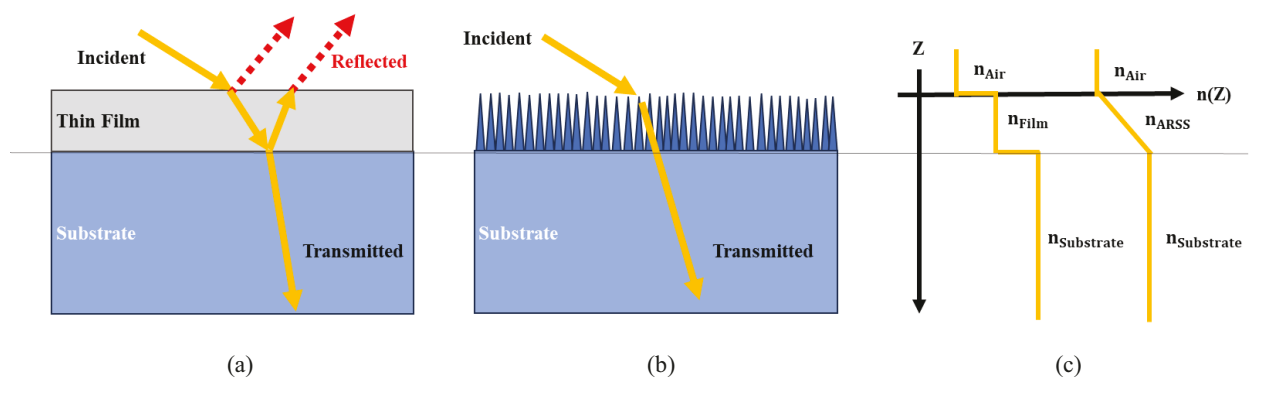


Figure 1. (a) Schematic of single layer anti-reflective thin film, compared to the same substrate containing (b) ARSS, and (c) refractive index profile for each with respect to propagation distance into the material. Appropriate thickness and thin film refractive index are required for reflected waves to destructively interfere. For ARSS, the index shift is gradual for subwavelength feature widths and periodicity therefore all diffraction orders higher than zero become evanescent, propagating only zero order transmission [6].

The laser induced damage threshold, LIDT or LDT, of ARSS on fused silica has been shown to be 10× that of thin-film AR and approaches the LDT of the bulk material for nanosecond pulse regime [7], and ultra-short-pulse laser (USPL) [8].

# 1.2 ARSS Fabrication Methods (Periodic vs Random)

Fabrication of high-aspect-ratio ARSS features on most materials and silica substrate requires a material removal process where an etch mask is deposited, then the substrate is etched away to generate monolithic structures. A standard photolithography process, like in the semiconductor industry, can be used to pattern an etch mask onto an optics surface. These are typically at periodic scales over one micron due to exposure equipment limitations, so this process is usually only suitable for ARSS in the infrared. Photolithography is also limited to inch-scale and flat optics. Random ARSS or rARSS, on the contrary, is scalable to large and curved optics and can exhibit broadband performance due to subtle variations in feature size and depth. Random ARSS can be fabricated by direct etching, without the use of mask, or using a thin, porous sputtered mask. The smaller feature sizes formed by rARSS are well suited for visible optics. Metal deposition, unlike photolithographic methods, has become an advantageous technique for fabrication of etching masks on large form factor optics [4].

A method to increase the size of rARSS to suit infrared optics involves a metal deposition and dewetting that generates quasi-periodic islands. This masking method has demonstrated the ability to tune the geometry, depth, and periodicity of the etch mask structures through variations in parameters such as deposition thickness and thermal annealing temperature [9,10]. These methods involved only one deposition and annealing step for etch mask formation.

Recently, a method for repetitive deposition and dewetting has been shown to allow for even broader tunability of the ARSS etch mask [6,9,11]. Metal deposition thickness and annealing temperature are the two main factors. The initial thickness before first annealing will set the feature periodicity. Additional steps of deposition and annealing will increase the size of the islands already present or "seeded". This increase in feature size allows for deeper etch depths translating to taller features, extending the gradual index change to perform AR at longer wavelengths. Figure 2 below gives a visual representation of how these metal masks surface features are generated through a repetitive process of deposition, annealing, and dewetting.

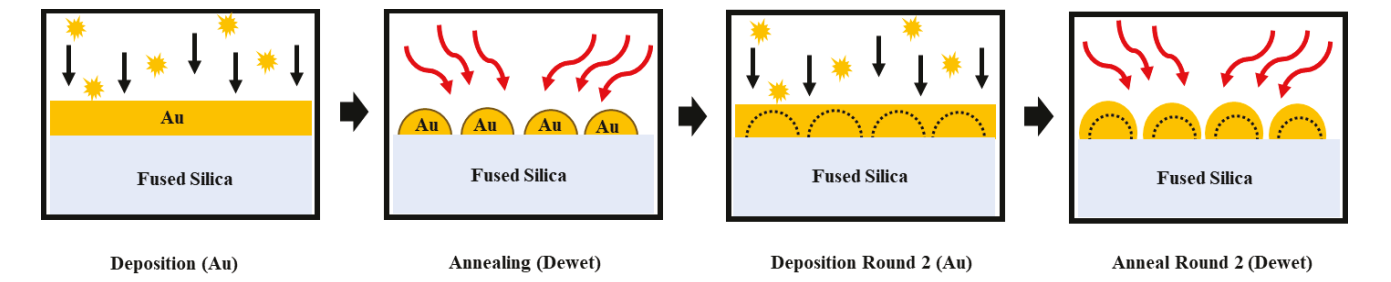


Figure 2. Schematic depicting the repetitive process of fabricating and reinforcing periodic metal mask surface structures onto substrate via deposition, annealing, and dewetting. The initial process will set the feature periodicity for the remainder of the steps. The figure illustrates formation of gold islands on a polished fused silica surface.

## 2. METHODS

#### 2.1 Mask and ARSS Fabrication

This study explores the seeded masking method and its tunability for ARSS performance. Fused silica (FS) and gold (Au) were chosen as the substrate and deposited metal, respectively. FS is used for a very large range of optical applications and Au has favorable surface tension and nanoparticle size. Additionally, its inherent resistance to oxidation enables diverse optical applications [11]. 1-inch-diameter, 0.0625-inch-thick double-sided polished silica windows were used (Quartz Plus, Inc., Brookline, NH, USA). Au was deposited on a rotating stage using a direct-current (DC) sputter deposition system (ACT 1800-F, AJA International, Inc., Hingham, MA, USA) with various nominal thicknesses of  $\sim$ 5, 10, and 15 nm on single side of the silica substrates. After deposition, annealing was performed at various peak temperatures from 300 to 500 °C (3/12 muffle furnace, Nabertherm GmbH, Lilienthal, Germany). A ramping time of  $\sim$ 15 minutes to reach peak temperature setting was used, then held for 10 minutes. The sample was cooled down ambiently until safe to handle. Heat initiates the dewetting process as the gold atoms detach from the substrate and bond together to form Au nanoparticles that accumulate into quasi-periodic islands while never fully reaching the Au bulk melting temperature of 1064 °C [6]. "Rounds" of repeated deposition and annealing were also performed with same settings as "seed" step or Round 1.

Once the desired Au mask was generated, the pattern was etched into the silica substrate via fluorine-based reactive ion etching (RIE 7000, PlasmaTherm, Inc., Saint Petersburg, FL, USA), until the Au was depleted. Figure 3 below contains images of the equipment used in fabrication throughout this study.

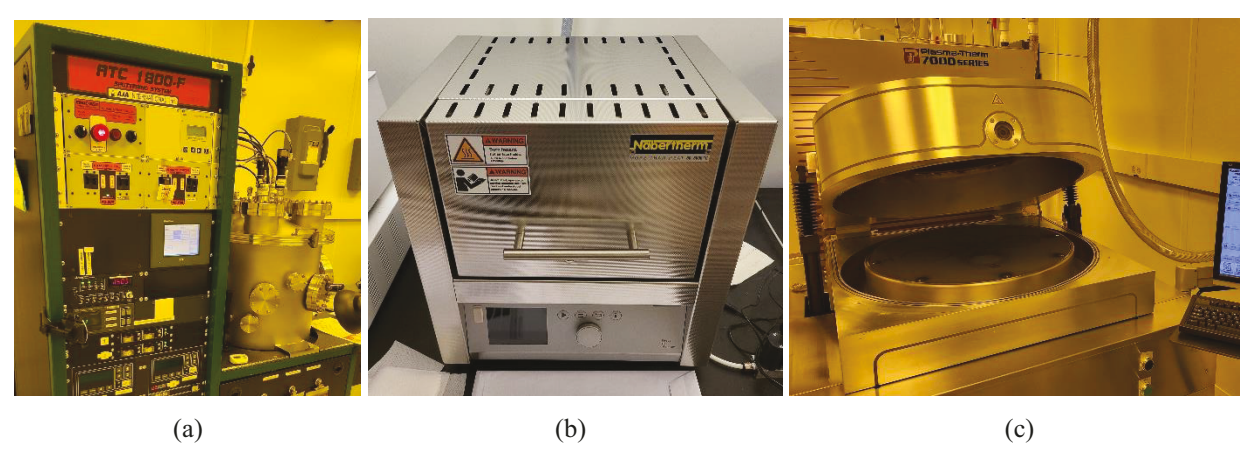


Figure 3. Primary equipment used for fabrication of rARSS on fused silica; (a) AJA deposition system, (b) Nabertherm muffle furnace, and (c) PlasmaTherm 7000 reactive ion etching system with 24-inch-diameter platen.

# 2.2 Performance Characterization and Feature Analysis

A comprehensive database of masking layer fabrication methods and resultant surface feature dimensions measured by scanning electron microscopy (150 SEM, Raith GmbH, Dortmund, Germany) as well as transmission spectra from wavelengths 200-1100 nm (CARY 60, Agilent Technologies, Inc., Santa Clara, CA, USA) were collected to track and analyze the Au dewetting process.

The SEM images (500 x 1000 pixels) at 50,000× magnification was first imported into MATLAB (MathWorks, Inc., Natick, MA, USA). The MATLAB Image Thresholder and Image Region Analyzer applications were used to convert the SEM grayscale image into a binary image. The binary image was used to determine three characteristics: fill factor, a measure of how much of the surface is covered by the masking material, average island equivalent diameter, and the island periodicity.

The fill factor was determined by calculating the total number of pixels that were over the threshold during binarization and dividing by the total number of pixels in the image.

Equivalent diameter was determined utilizing the MATLAB Image Region Analyzer application. The island segmentation was performed with 8-connectivity, "regionprops" function, so that any two adjacent pixels are considered part of one island. The number of connected pixels for each island, excluding islands of ~5-10 pixels or less, and an area calculation consisting of the number of pixels in each region was also listed. The equivalent diameter (in pixels) was then determined based on the diameter of a circle with the same area (number of pixels) as the region of interest, calculated by rearranging the area equation for a circle.

To determine the island periodicity, the centroid of each island on the new list was calculated and cataloged as a point on the x-y plane. Then for each point, the distance to the nearest other centroid was found and listed. Both the average and the standard deviation of these distances were scaled and used as a radius for the following step. For each centroid, the distance to all neighboring centroids within the radius was found, averaged, and listed. The average of these averages was taken to be the island periodicity. The periodicity as the average Euclidian distance between each island and its neighbors, averaged over all islands. Where n is the total number of islands, and m is the islands whose centroid is within a radius for each n.

$$\frac{1}{n}\sum_{i=1}^{n} \frac{1}{m}\sum_{j=i}^{m} \sqrt{(x_i - x_j)^2 + (y_i - y_j)^2}$$
 (1)

All analysis was initially calculated in pixels and converted to nm based on the scale bars present within the SEM images. The conversion was determined to be  $\sim$ 2.22 nm per pixel.

## 3. RESULTS AND DISCUSSION

First, a comparison of initial Au deposition thickness to dewetted Au islands was performed. While various annealing temperatures were studied, Figure 4 (top row) shows SEM images collected for a single maximum temperature. Island size and spacing is shown to increase with increasing initial Au deposition thickness. These island masks were then etched in the plasma chamber for various durations, coinciding with the depletion of the Au mask. Figure 4 (bottom row) shows SEM images at normal incidence of the etched FS surface.

The ARSS lateral feature dimensions for the 10 and 15 nm initial deposition thicknesses appear to match well compared to their masks. The 5 nm initial deposition and dewetted islands were much smaller compared to the ARSS features transferred to the FS after etching. Our speculation is the inherent heat in the plasma etching process further annealed the mask while etching. For all the etches performed with this glass, there appeared to be a minimum ARSS pillar or feature width, regardless if the island mask used had smaller dimensions. Any ARSS with features smaller than shown in Figure 4 (bottom left) were not pillars, but instead holes.

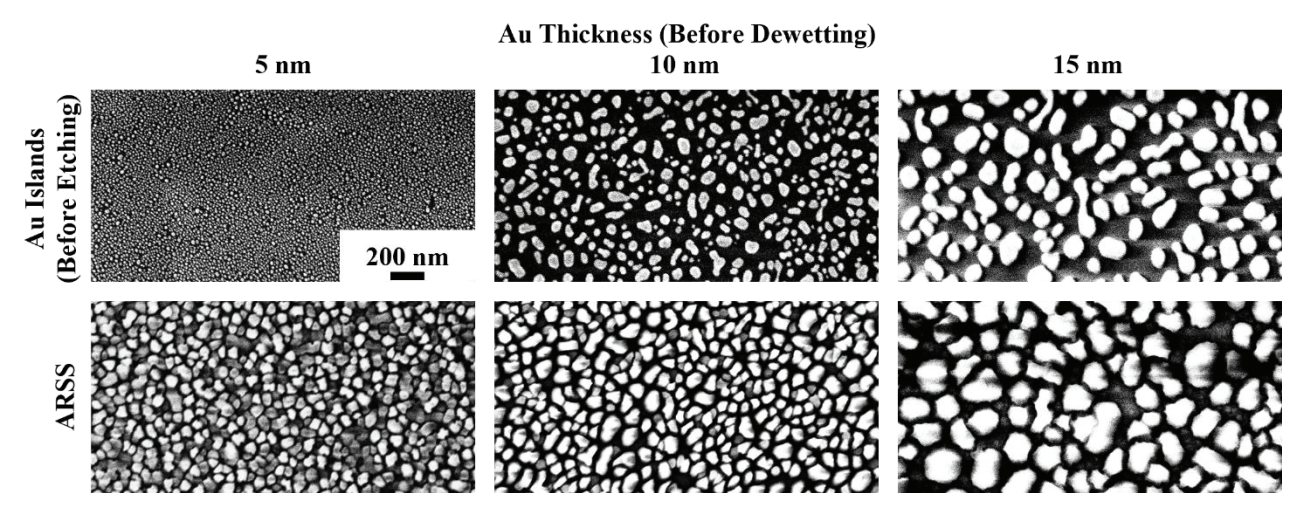


Figure 4. Scanning electron microscope (SEM) images of Au island masks, and corresponding ARSS etched into fused silica, for three different initial deposition thicknesses (5, 10, and 15 nm). Images were taken at 50,000× magnification.

The optical transmission of these three ARSS samples were measured and shown compared to polished blank sample in Figure 5. The blank FS sample has two main Fresnel reflection losses from the front and back surface. Therefore, a theoretical maximum single-side AR enhancement was approximated as the square-root of the double-side polished blank sample, shown in gray in Figure 5. The peak transmission enhancement was measured in the ultraviolet, visible, and infrared for the initial deposition thicknesses of 5, 10, and 15 nm, respectively. The limited range of our spectrometer did not capture the exact maximum of the 15 nm sample. For the visible regime, the 10 nm mask thickness showed a broadband enhancement with a peak transmission around  $\lambda$ =650 nm, 97% of the theoretical maximum.

The larger the ARSS features, the more scattering occurs and dominates the loss in transmission at shorter wavelengths. However, larger mask features allow for deeper etching and taller ARSS pillars to increase transmission at longer wavelengths. ARSS shown was etched with same etch chemistry and until Au mask depletion.

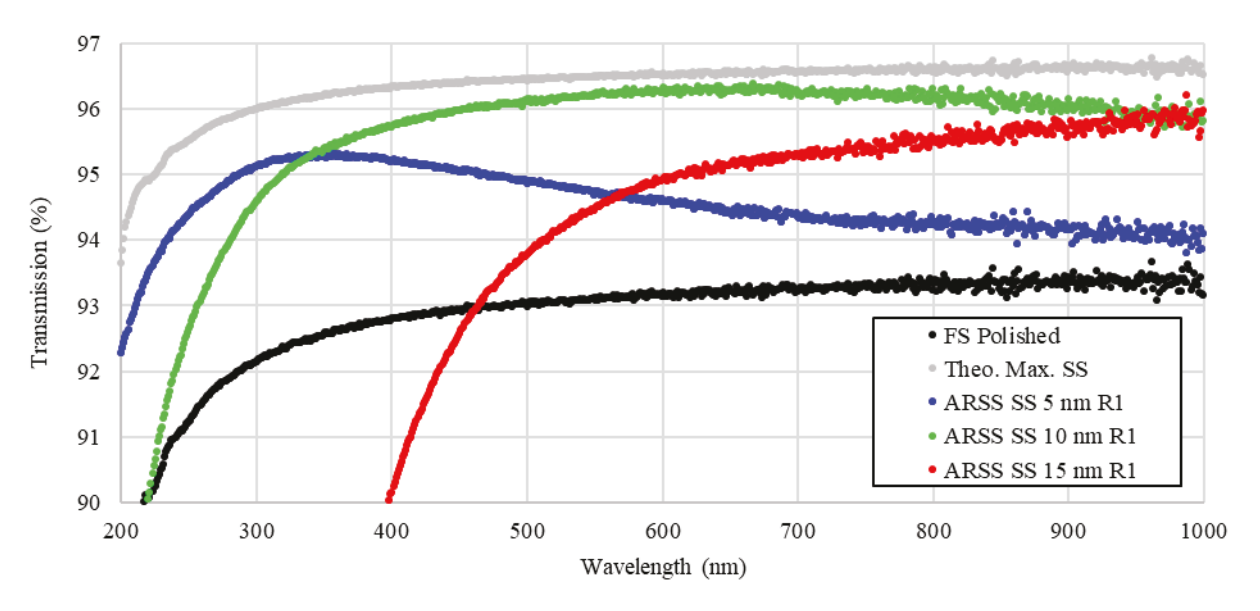


Figure 5. Measured transmission (%T) of single-sided (SS) ARSS on FS with three dewetted island masks for 1 round. The measurements were taken at normal incidence and the mask annealing temperature was uniform.

Next, the effects of repeated deposition and annealing were explored. The three initial deposition thicknesses of 5, 10, and 15 nm were annealed, and imaged via SEM. The same Au initial thickness or deposition duration was then deposited over the once annealed islands, and annealed again, as illustrated in Figure 2. This process was repeated for up to 4 rounds.

While various annealing temperatures were studied, Figure 6 shows SEM images collected for a single maximum temperature for direct comparison. Table 1 contains the analytical results from analyzing the SEM images in Figure 6. The mean of all round periodicities for the same initial deposition thickness is shown in left column of Table 1.

The results show that each iterative step of deposition and annealing correlates with an increasing fill factor for the mask features on the substrate, while still maintaining the periodicity established by the seed or first dewetting process.

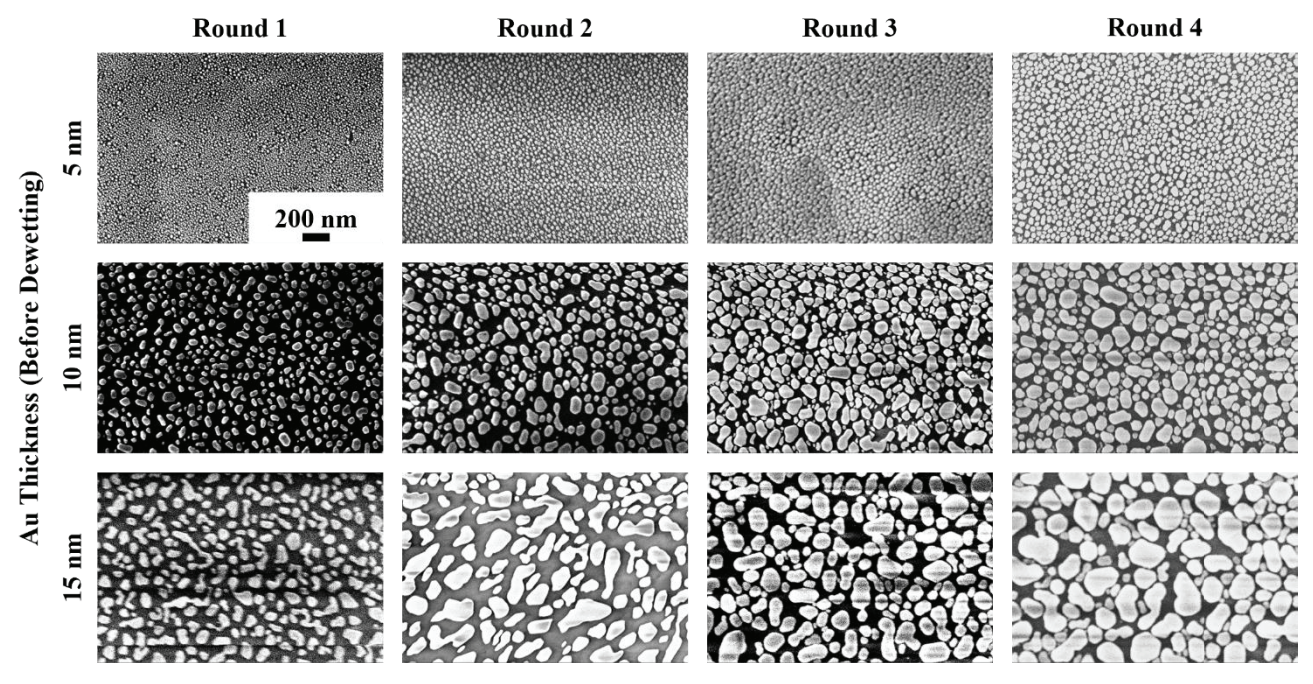


Figure 6. Scanning electron microscope (SEM) images of multiple rounds of Au mask fabrication on FS substrate for initial and subsequent deposition thicknesses of 5, 10, and 15 nm. The columns represent the iterative steps or rounds 1-4 of deposition and annealing. The rows represent the amount of Au redeposited for each round. The images are of the same scale and were taken at 50,000× magnification. Some imaging artifacts can be seen, due to charging of the non-continuous conductive surface.

Table 1. Island mask parameters obtained via image analysis.

	Round	Avg. Equivalent Dia. (nm)	Periodicity (nm)	Fill Factor
Dep. Thickness	1	12	23	10 %
Per Round:	2	18	35	24 %
5 nm Periodicity:	3	26	44	33 %
$34 \pm 9 \text{ nm}$	4	34	34	50 %
Dep. Thickness	1	44	94	28 %
Per Round:	2	62	96	39 %
10 nm Periodicity:	3	61	90	47 %
91 ± 6 nm	4	79	84	49 %
Dep. Thickness	1	72	80	28 %
Per Round:	2	120	165	37 %
15 nm Periodicity:	3	116	122	47 %
$131 \pm 39 \text{ nm}$	4	111	159	48 %

It is worth noting, that the only results that did not follow the trend of stable periodicity were the 15 nm deposition rounds. Annealing temperature is a determining factor in the efficiency of the island formation, where higher deposition thicknesses required higher temperatures to generate circular Au islands. However, even at the lower annealing temperature the increasing fill factor trend still held true.

Analysis of the surface features present during each step of this iterative process shows a trend of increasing fill factor and average diameter, while roughly maintaining the island spacing or periodicity. For ARSS, the short end scattering edge wavelength is related to the feature sizes, while the transmission enhancement is related to the depth of the etch or features. Taller features extend the gradient-like refractive-index effect, suppressing reflection. This is seen in Figure 7 where the measured transmission spectra for masks of the same periodicity but increasing island size and fill factor correlates to shifts in the scattering edge of the spectral transmission curve to higher wavelengths, before Au mask depletion.

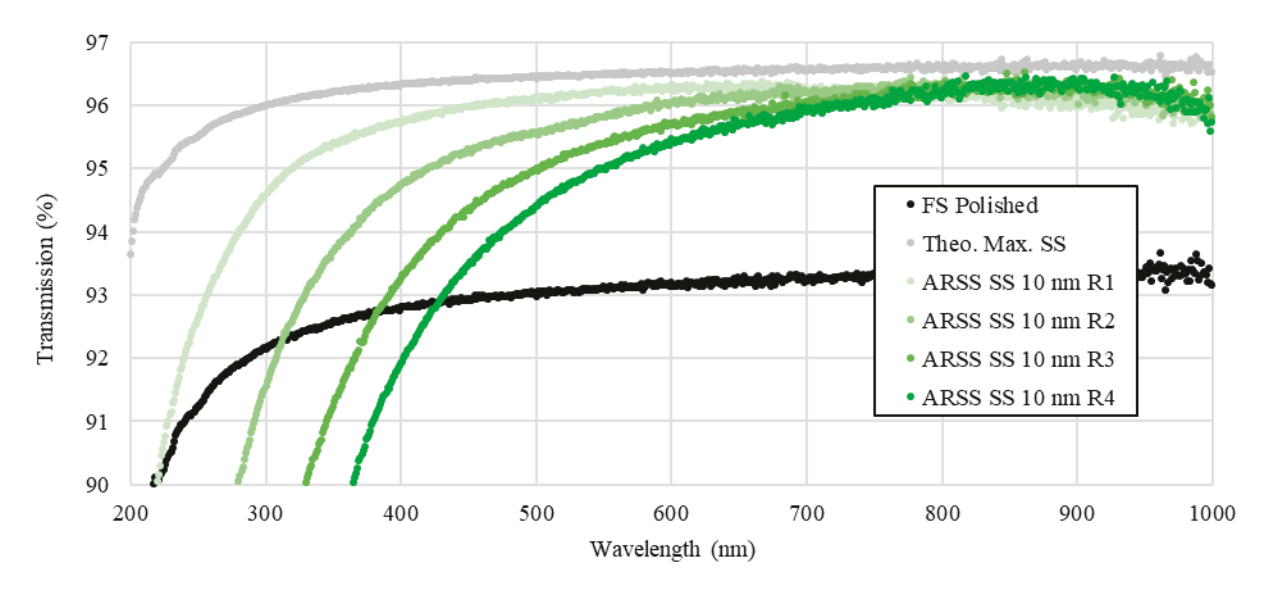


Figure 7. Measured transmission enhancement (%T) resulting from etching fused silica substrates with ARSS on single surface. Five examples are shown, a blank, polished sample, and four etched samples of 10 nm Au deposition thickness, with each sample having an addition round of deposition and annealing. The measurements were taken at normal incidence and the annealing temperature was uniform. The theoretical maximum transmission for a single side processed sample is shown. Each additional round shifts the scattering edge and peak transmission to higher wavelength.

Tunability of specific wavelength transmission capabilities on the scale of tens to hundreds of nanometers is achievable through this method of metal mask fabrication. Etching these masked samples resulted in broadband transmission enhancement that can be applied to many different extremely specified applications.

While only a limited case is presented, there is an array of dewetted mask and etching parameters to explore further. Varying deposition thicknesses and annealing temperature between rounds, would allow for vast array of masking possibilities. There are instances where comparable masks could be formed with one method requiring less rounds and overall fabrication time. Adjustable chemistry and etching chamber parameters also provide opportunities to realize high performance ARSS from these masks. More exploration and optimization is needed. A major benefit of this controlled masking method is the scalability to large diameter and thick optics, often not practical with photo-lithography methods.

# 4. CONCLUSIONS

Experimental results from the fabrication of Au features on smaller optics can be transferred to large scale optics where invasive imaging/analysis of metasurface features are not readily available. From these Au masking results, we can correlate the SEM images and transmission spectra produced from these small optic samples to verify masking on larger optics with consistency and confidence. For an initial deposition thickness of 10 nm and repeated iterative steps of deposition and annealing, the fill factor increased (28%, 39%, 47%, 49%), while the island periodicity was maintained at

average 91 ± 6 nm for all iterative steps. Etching these masked samples resulted in broadband transmission enhancement, over 94% of theoretical maximum. A comprehensive database of masking layer fabrication, resultant surface feature dimensions, and ARSS transmission enhancement capabilities was generated. This scalable masking approach can broaden high laser damage threshold applications utilizing tunable performance anti-reflective structured surfaces (ARSS).

## **ACKNOWLEDGEMENTS**

We acknowledge primary financial support by ONR award N00014-22-1-2623 and N00014-24-1-2138. Also, NSF within the I/UCRC for Metamaterials (2052745), the Center for Optoelectronics and Optical Com. at the College of Science of UNC Charlotte. The PlasmaTherm RIE 7000 was supported by ONR DURIP. The authors would also like to thank the UNC Charlotte Optics Center staff specifically Scott Williams, Daniel Furr, and Lou Deguzman for their facilities and equipment support.

## REFERENCES

- [1] Stolz, C. J., & Negres, R. A., "Ten-year summary of the Boulder Damage Symposium Annual Thin Film Laser Damage Competition," Optical Engineering, 57(12), (2018).
- [2] Schubert, M. F., Poxson, D. J., Mont, F. W., Kim, J. K., & Schubert, E. F., "Performance of antireflection coatings consisting of multiple discrete layers and comparison with continuously graded antireflection coatings," Applied Physics Express, 3(8), 082502 (2010).
- [3] Carr, C. W. et. al., "Localized dynamics during laser-induced damage in optical materials," Physical Review Letters, 92(8), (2004).
- [4] Ray, N. J., et. al., "Designer metasurfaces for antireflective applications enabled by Advanced Nanoparticle Technology," Advanced Optical Materials, 10(10), (2022).
- [5] Seungmuk, J., et al. "Improved antireflection properties of moth eye mimicking nanopillars on transparent glass: Flat antireflection and color tuning," Nanoscale, 4(15), 4603-4610, (2012).
- [6] Raguin, D. H., & Morris, G. M., "Antireflection structured surfaces for the Infrared Spectral Region," Applied Optics, 32(7), 1154, (1993).
- [7] Wilson, C. R., et. al., "Laser damage of silica optical windows with random antireflective structured surfaces," Opt. Eng. 57(12), 121906 (2018).
- [8] Busse, L. E. et al., "Ultrashort Pulse Laser Irradiation Tests on Silica Glass with Random Antireflective Surface Structures," Conference on Lasers and Electro-Optics (CLEO), pp. 1-2 (2018).
- [9] Ray, N. J., et. al., "Substrate-engraved antireflective nanostructured surfaces for high-power laser applications," Optica 7, 518-526 (2020).
- [10] Eckart A. P., et. al., "Control of spectral transmission enhancement properties of random anti-reflecting surface structures fabricated using gold masking," Proc. SPIE 10115, Advanced Fabrication Technologies for Micro/Nano Optics and Photonics X, 101150B (2017).
- [11] Ray, N. J., et. al., "Enhanced tunability of gold nanoparticle size, spacing, and shape for large-scale plasmonic arrays," ACS Applied Nano Materials, 2(7), 4395–4401, (2019).